

Efficient Decoder for End-to-End Oriented Object Detection in Remote Sensing Images

Jiaqi Zhao, Zeyu Ding, Yong Zhou, Hancheng Zhu, Wenliang Du, Rui Yao, *Member, IEEE*,
and Abdulmoteleb El Saddik, *Fellow, IEEE*,

Abstract—Object instances in remote sensing images often distribute with multi-orientations, varying scales, and dense distribution. These issues bring challenges to end-to-end oriented object detectors including multi-scale features alignment and a large number of queries. To address these limitations, we propose an end-to-end oriented detector equipped with an efficient decoder, which incorporates two technologies, Rotated RoI attention (RRoI attention) and Selective Distinct Queries (SDQ). Specifically, RRoI attention effectively focuses on oriented regions of interest through a cross-attention mechanism and aligns multi-scale features. SDQ collects queries from intermediate decoder layers and then filters similar queries to obtain distinct queries. The proposed SDQ can facilitate the optimization of one-to-one label assignment, without introducing redundant initial queries or extra auxiliary branches. Extensive experiments on five datasets demonstrate the effectiveness of our method. Notably, our method achieves state-of-the-art performance on DIOR-R (67.31% mAP), DOTA-v1.5 (67.43% mAP), and DOTA-v2.0 (53.28% mAP) with the ResNet50 backbone.

Index Terms—Oriented object detection, remote sensing images, end-to-end detectors, attention.

I. INTRODUCTION

ORIENTED object detection aims to predict categories and a set of oriented boxes for each target and is widely applied in remote sensing images. Unlike horizontal object detection towards to natural scene, oriented object detection is still a challenging task due to the variety of oriented objects, e.g. arbitrary orientation, varying scales, and dense distribution. Moreover, modern oriented detection methods have achieved excellent results based on convolutional neural networks (CNNs). These methods can be divided into two types: single-stage [1], [2] and two-stage methods [3], [4]. Single-stage methods benefit from numerous anchors (position prior) and a simple architecture. Two-stage methods are trained by a coarse-to-fine style intrinsically to learn abundant features.

Zeyu Ding, Yong Zhou, and Rui Yao are with the School of Computer Science and Technology, China University of Mining and Technology, Xuzhou 221116, China, and also with the Engineering Research Center of Mine Digitization, Ministry of Education of the People's Republic of China, Xuzhou 221116, China (e-mail: dingzeyu@cumt.edu.cn; yzhou@cumt.edu.cn; ruiyao@cumt.edu.cn).

Jiaqi Zhao is with the Engineering Research Center of Mine Digitization, Ministry of Education of the People's Republic of China, Innovation Research Center of Disaster Intelligent Prevention and Emergency Rescue, School of Computer Science and Technology, China University of Mining and Technology, Xuzhou 221116, China (e-mail: jiaqizhao@cumt.edu.cn).

Abdulmoteleb El Saddik is with the School of Electrical Engineering and Computer Science, University of Ottawa, Ottawa, ON K1N 6N5, Canada (e-mail: elsaddik@uottawa.ca).

Digital Object Identifier

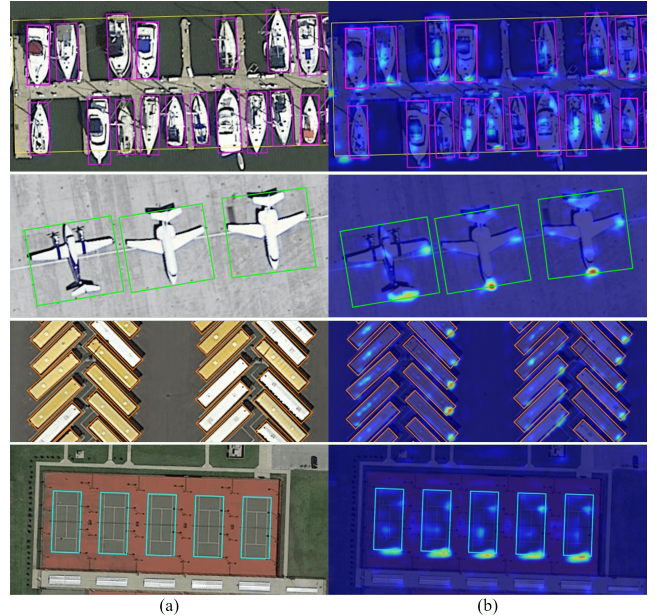


Fig. 1. (a) Object instances in remote sensing images exhibit arbitrary orientation, different scales and dense distribution. (b) Visualization of RRoI attention without using CAM. RRoI attention align features and mostly attends to object extremities such as the front and back of ships, planes and vehicles.

Inspired by the attention and transformer in natural language processing (NLP) [5], many detectors introduce it into horizontal object detection to extract global features and show promising performance [6], [7]. Most end-to-end horizontal object detectors rely on an encoder-decoder framework and remove complicated hand-designed modules.

However, when the end-to-end framework is integrated into oriented object detection, it will suffer from several challenges. First, *objects appear in arbitrary orientations leading to misalignment between features and oriented boxes*, shown in Fig. 1(a). Image features as values and oriented boxes as positional queries need to be aligned when they are interacted with in cross-attention. Second, *the scales of objects in remote sensing is varying*, shown in Fig. 1(a). Small and large objects require high and low resolution features respectively. Multi-scale features are necessary to adapt objects of different scales. Third, *dense objects require a large number of queries*. In remote sensing scenes [8], it's common to find hundreds of densely packed object instances within a single image. In contrast, images in natural datasets [9] typically contain no more than one hundred objects, e.g. in the COCO dataset [9],

nearly 99% of the images have fewer than 30 objects. So, 100 queries in DETR [6] are sufficient, but they are still fewer than the objects in some remote sensing images. To enhance performance, some horizontal detectors [10], [11] have increased the number of queries by more than 1000. However, if we apply the same rate of increase to remote sensing queries, computation overhead will be increased significantly. Last, *similar queries hinder optimization*. The end-to-end detectors adopt one-to-one label assignments. Consider the situation where two queries are entirely identical. When label assignment, one query is assigned as a positive sample, while the other is assigned as a background category. Such a problem can potentially introduce adverse effects into the training process [12].

In this paper, we propose an end-to-end oriented object detector to address the above problems called Rotated RoI Transformer (RRoIFormer), which consists of two effective technologies, Rotated RoI attention (RRoI attention) and Selective Distinct Queries (SDQ). Specifically, the proposed RRoI attention can align image features with oriented objects through an attention mechanism. Learnable oriented boxes as positional queries extract aligned features which serve as the values in this attention mechanism. Content queries generate attention weights and aggregate the values naturally. The features around the center point of oriented boxes and within them are highlighted and scored by the attention mechanism, shown in Fig. 1(b). The time complexity of RRoI Attention is of a similar magnitude to deformable attention [7].

In addition, our proposed Selective Distinct Queries (SDQ) collects queries from intermediate decoder layers once and then filters similar queries to obtain distinct queries. In modern end-to-end detectors, the decoder consists of 6 consecutive decoder layers [7], [12], [13] and each decoder layer predicts results supervised by loss functions. We have observed that queries in the intermediate layers can represent objects adequately compared to initial queries. Hence, we collect queries from intermediate layers as high-quality selective queries, without introducing a large number of initial queries [10] or extra auxiliary network branches [11], [14]. But there are a large number of similar queries [12] within the query set. These similar queries hinder the optimization of training. Our proposed method can significantly filter similar queries and keep the remaining queries distinct, which facilitates one-to-one label assignment and training. The number of distinct queries is dynamic and normally less than the initial ones. SDQ is embedded into intermediate decoder layers, rather than positioned before or after the entire decoder.

Our contribution can be summarized in three-folds:

- The Rotated RoI attention is proposed to align multi-scale image features and oriented boxes via a cross-attention mechanism for objects with arbitrary orientations and varying scales towards oriented object detection tasks.
- To avoid a large number of initial queries or extra branches, the proposed Selective Distinct Queries first collects sparse high-quality queries from the intermediate decoder layers. Second, it filters similar queries to obtain distinct queries, which can facilitate one-to-one label assignment and training.

- Extensive experiments demonstrate the effectiveness of our approach. With the Resnet50 backbone, RRoIFormer achieves an mAP of 67.31% on DIOR-R, 67.43% on DOTA-v1.5, and 53.28% on DOTA-v2.0 respectively, establishing new state-of-the-art benchmarks.

II. RELATED WORK

A. Attention in Object Detection

DETR [6] first introduces Transformer [5] into object detection, but the single feature map and vanilla attention are low efficiency to scale and large resolution images. The spatially modulated co-attention proposed in SMCA [15] combines vanilla attention with a Gaussian-like weight map to constrain co-attention to focus more on regions near the predicted box. The deformable attention modules proposed by Deformable DETR [7] only focus on some key sampling points around a reference. These key sampling points are responsible for both classification and regression, but at the supervision of orientation, they are located at special positions that are sub-optimal, like the catercorner and axis of boxes. Anchor DETR [16] designs Row-Column Decoupled Attention that performs the row attention and column attention successively. The decoupled row and column attention loses spatial and orientation information. Some works [17], [18] realize attention using dynamic convolution [19], [20]. Different from above attentions, our proposed Rotated RoI attention (RRoI attention) focus on interested regions of learnable boxes $B(x, y, w, h, \theta)$ distributed in multi-scale features and align the multi-scale features to oriented objects. The time complexity of RRoI Attention is the same order of magnitude as deformable attention.

B. Methods of Query Update

We classified current methods of query update into three types: the basic type, query enhancement type, and auxiliary decoder branch type. In all these types, queries are successively updated layer by layer in the decoder. In the basic way, a fixed number of queries which are initialized randomly are fed into the first decoder layer and the outputs are also the same number of initial queries. Subsequently, these queries are decoded successively by other decoder layers, each sharing the same structure [6], [7], [13]. Due to the sparsity and random initialization of the queries, some enhancement methods are proposed. Anchor DETR [16] attaches three patterns to each anchor point which enlarge query numbers. Dynamic Sparse R-CNN [21] replaces random initialization with a dynamic proposal generation mechanism to initialize proposals and features. DDQ [12] supervises dense boxes lying on features and selects top-scoring distinct proposals as inputs to the decoder. SQR [22] stacks queries from previous decoder layers and feeds them to later layers. DQ-Det [23] combines basic queries as modulated queries according to the convex combination. Some researchers introduce an auxiliary decoder branch to accelerate training convergence. To realize one-to-many label assignment, Group DETR [24] feeds multiple groups of queries to decoders as auxiliary branches in parallel, similar to the way in H-DETR [11]. DN-DETR [25] and

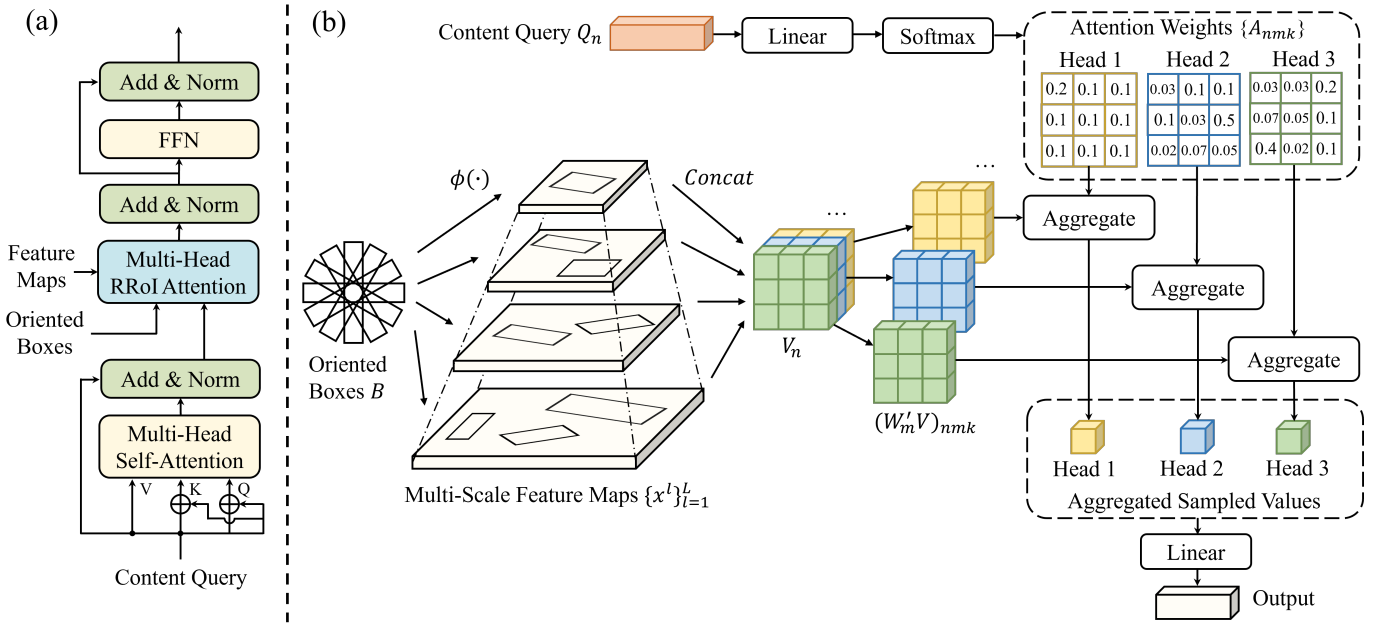


Fig. 2. Rotated RoI attention. (a) Decoder with Rotated RoI attention. (b) Rotated RoI attention.

DINO [10] add noises to bounding boxes and class labels as noising queries in an auxiliary branch to mitigate the instability of bipartite graph matching. Co-DETR [14] train multiple auxiliary heads supervised by one-to-many label assignments, such as ATSS [26] and Faster R-CNN [27]. Different from the above query learned way, our Selective Distinct Queries (SDQ) collects sparse high-quality queries from intermediate decoder layers which avoid a large number of initial queries or auxiliary decoder branches. To facilitate one-to-one label assignment, SDQ filters similar queries and obtains distinct queries. Moreover, SDQ is embedded among decoder layers, rather than served as an auxiliary head. Without losing generality, SDQ can be easily combined with other enhancement methods.

III. PROPOSED METHOD

In this paper, we propose an end-to-end oriented detector called RRoIFormer which is equipped with an efficient decoder. We first introduce the architecture in Sec. III-A. Specifically, we illustrate the Rotated RoI attention (RRoI attention) and Selective Distinct Queries (SDQ) in Sec. III-B and III-C respectively.

A. Overall Architecture

Our RRoIFormer consists of a backbone and an efficient decoder shown in Fig. 2(a), where we use multi-scale feature maps to represent the backbone for brevity. Multi-scale features are extracted by backbone (e.g., ResNet50 [28], SwinTransformer [29]) and Feature Pyramid Network (FPN). Images in remote sensing scenes are very huge which leads to a large size of corresponding image features. To reduce the computational overhead, we do not introduce the encoder to further interact with features following [30]–[32]. The efficient

decoder incorporates two technologies, Rotated RoI attention (RRoI attention) and Selective Distinct Queries (SDQ). The decoder consists of multiple successive decoder layers. Queries generated from every decoder layer are assigned by a one-to-one label assignment strategy and supervised by the same losses. Classification for categories and regression for positions of objects are two tasks in oriented object detection.

B. Rotated RoI Attention

Decoder with Rotated RoI Attention. Both cross-attention and self-attention modules are in the decoder shown in Fig. 2(a). A small set of learnable content queries $Q \in \mathbb{R}^{N \times C}$ are high-dimension (e.g., $C = 256$) latent vectors and are expected to encode semantic information of objects. For brevity, we use queries to represent content queries below. The positional encoding embeddings are randomly initialized with the same shape as queries and then added by queries following [6]. The queries and positional encodings are jointly trained with the networks. In self-attention modules, queries interact with each other and the outputs keep the same shapes as the inputs. In our proposed Rotated RoI attention, as cross-attention, queries interact with corresponding regions of aligned features. The inputs of RRoI attention include queries from self-attention, learnable oriented boxes as positional queries, and multi-scale feature maps. Though the queries represent object characteristics, we introduce learnable oriented boxes $B \in \mathbb{R}^{N \times 5}$ to localize the objects. These oriented boxes are represented by parameters (x, y, w, h, θ) , denoting the center coordinate, width, height, and angle, respectively. The number of oriented boxes always equals queries. Both queries and oriented boxes are initialized randomly as learnable embeddings [6], [13], [33] or come from enhancement modules [7], [12], [16], [21]. The multi-scale feature maps $\{x^l\}_{l=1}^L$, where $x^l \in \mathbb{R}^{C \times H_l \times W_l}$, are extracted by backbone (e.g., ResNet50 [28], SwinTrans-

former [29]) and Feature Pyramid Network (FPN). In the next section, we will discuss RRoI Attention modules specifically.

Multi-Scale Rotated RoI Attention Module. Given oriented boxes $B \in \mathbb{R}^{N \times 5}$ and multi-scale feature maps $\{x^l\}_{l=1}^L$ in Fig. 2(b), to solve the misalignment problems, we first align the features as values V ,

$$V = \text{Concat}\{R_l(x^l, \phi(B_n), r)\}_{n=1}^N \quad (1)$$

where integer l index the input feature level, and n index the oriented boxes. Function $\phi(B_n)$ maps oriented boxes to different feature levels by their scales. Function $R_l(\cdot)$ warps region features from the corresponding feature x^l precisely according to oriented boxes and pooling size r , e.g. Rotate RoI Align [34]. Next, the values $V \in \mathbb{R}^{N \times C \times r^2}$ will further interact with queries. Given queries $Q \in \mathbb{R}^{N \times C}$, the multi-scale Rotated RoI Attention is calculate by

$$\text{MSRRoIAttn}(Q_n, B_n, \{x^l\}_{l=1}^L, r) = \sum_{m=1}^M W_m \left[\sum_{k=1}^{r^2} A_{nmk} \cdot (W'_m V)_{nmk} \right] \quad (2)$$

where n indexes the oriented boxes and queries, m indexes the attention heads and k indexes all r^2 points at a single value map. The attention weight A is obtained via linear projection over the queries. Specifically, the queries Q are first fed to a linear projection operator of $M \times r^2$ channels and then are fed to a softmax operator to obtain the attention weight $A \in \mathbb{R}^{N \times M \times r^2}$. A_{nmk} denotes the attention weight of the k^{th} point at a single value map in the m^{th} head. The scalar attention weight A_{nmk} is normalized by $\sum_{k=1}^{r^2} A_{nmk} = 1$. The W'_m and W_m are input value projection and output projection matrix at m^{th} head respectively.

Complexity For Rotated Rotated RoI Attention. When calculating the values, to align features for oriented boxes, the bilinear interpolation will be used. Four adjacent pixel values interpolate one precise target point. So the complexity for calculating values is $O(4Nr^2s)$, where s denotes the sampling ratio and r^2s denotes all sampling points in one oriented box. Then for projecting values to multiple heads, the complexity is $O(r^2NC^2)$. Due to attention weights obtained via linear projection over queries, the complexity is $O(MNCr^2)$. When attention weights and values interact, it is $O(NCr^2)$. Finally, for aggregating sampled values, the complexity is $O(NC^2)$. So the overall complexity of Rotated RoI attention is $O(4Nr^2s + r^2NC^2 + NMCr^2 + NCr^2 + NC^2)$. In our experiments, $M = 8$, $r = 7$, $s = 4$ and $C = 256$ by default, thus $r^2 < C$ and the complexity is of $O(N(50C^2 + 441C + 784))$.

C. Selective Distinct Queries

Basic Query Update in Decoder. Before the first decoder layer, the queries and oriented boxes are initialized as inputs to the decoder, shown in Fig. 3(a). For brevity, both initial queries and oriented boxes are denoted by $q^0 = \{q_1^0, q_2^0, \dots, q_n^0\}$ here. In the basic query update mode, there are d identical decoder layers (e.g. $d = 6$) stacked successively. Each decoder layer D^i takes the queries q^{i-1} from the previous layer and processes them to obtain the updated queries q^i for the next layer,

$$q^i = D^i(q^{i-1}) \quad (3)$$

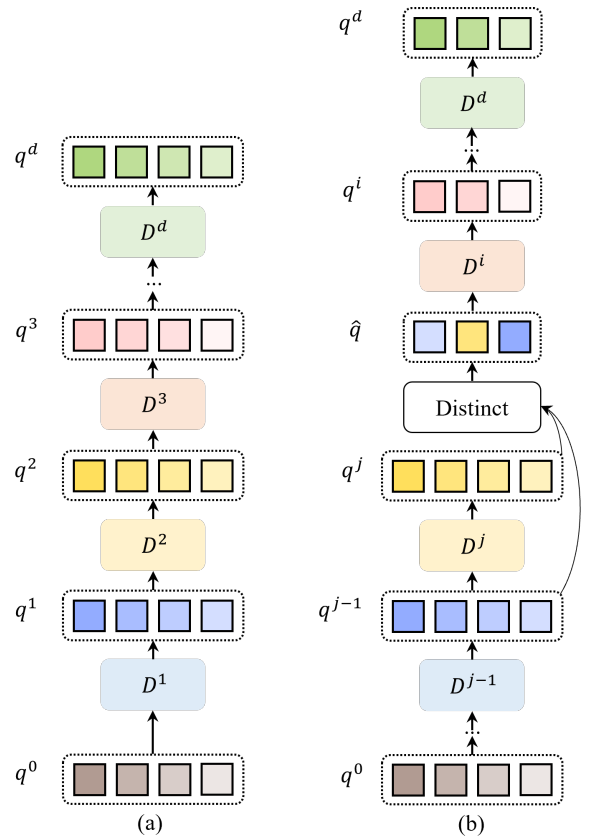


Fig. 3. (a) Basic process for queries update layer by layer in decoder. (b) Selective Distinct Queries.

TABLE I

MAP RESULTS IN DIFFERENT DECODER LAYERS. SPARSE R-CNN (100 QUERIES) WITHOUT RANDOM RESIZE DATA PROCESSING ARE TRAINED ON COCO TRAIN SET AND PER LAYER MAP IS REPORTED ON VALIDATION SET.

Model	D^1	D^2	D^3	D^4	D^5	D^6
Sparse R-CNN	14.1	31.6	39.7	43.7	44.7	45.0

where $i = 1, 2, \dots, d$ and d is the total number of decoder layers. After passing through all decoder layers, the model would typically have generated refined queries q^d . The loss $\mathcal{L} = \lambda_{cls} \mathcal{L}_{cls} + \lambda_{L_1} \mathcal{L}_1 + \lambda_{iou} \mathcal{L}_{iou}$ is applied at the queries of all the decoder layers for training, where \mathcal{L}_{cls} is the focal loss [35] for classification, \mathcal{L}_1 and \mathcal{L}_{iou} are L1 Loss and Rotated IoU/GIoU Loss [36], [37] for regression.

Selective Queries. As shown in Table I, it appears that there is a clear growing trend in mAP as queries move deeper into the decoder layers. Notably, the mAP for the last few layers is very close to each other. Take Sparse R-CNN as an example, the mAP is 43.7%, 44.7% and 45.0% at the 4th, 5th and 6th decoder layer respectively. This suggests that the queries in the last few decoder layers already capture sufficient information about object positions and categories. Therefore, we can collect the queries from p intermediate decoder layers as selective queries only once and similar queries among them will be filtered to obtain distinct queries in the next step, shown

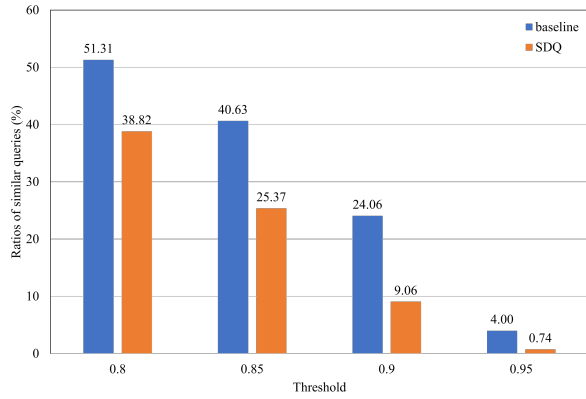


Fig. 4. The ratios of similar queries under different high IoU threshold. Compared with baseline, SDQ significantly remove similar queries.

in Fig. 3(b).

$$q^p = \text{Concat}(q^j, q^{j-1}, \dots, q^{j-p-1}) \quad (4)$$

where q^p denotes as selective queries from the j^{th} , $(j-1)^{\text{th}}$, \dots , $(j-p-1)^{\text{th}}$ intermediate decoder layers, totally p layers. The number of selective queries is $p \times n$, where n is the initial number of queries. Different p intermediate decoder layers collect p times initial queries. These selective queries avoid a large number of initial queries and multiple auxiliary branches.

Distinct Queries. The selective queries collected from intermediate decoder layers already capture sufficient information about the positions and categories with the images. But there exist many similar queries. To obtain distinct queries, similar queries will be filtered,

$$\hat{q} = \begin{cases} \text{top-}n(\psi(q^p)), & |\psi(q^p)| > n \\ \psi(q^p), & |\psi(q^p)| \leq n \end{cases} \quad (5)$$

where \hat{q} denotes distinct queries. Distinct queries are calculated in two steps. First, we filter similar queries by a simple class-agnostic non-maximum suppression (NMS), denoted as $\psi(\cdot)$. Second, if the remaining queries $\psi(q^p)$ are more than the initial queries n , we will choose the first n ones according to scores as distinct queries. Otherwise, all remaining queries are treated as distinct queries. The class-agnostic NMS operation here is regarded as the first step of distinct queries mechanisms embedded among intermediate decoder layers, instead of as post-processing at the inference stage in traditional detectors [3], [4]. Therefore, such a method still conforms to the end-to-end standard. In the basic queries update way, the last decoder layer D^d exclusively refines queries from the D^{d-1} , while our method handles queries from multiple intermediate layers simultaneously. Through filtering similar queries, the number of distinct queries is reduced which reduces computational overhead.

Analysis of Selective Distinct Queries. Our proposed SDQ can filter similar queries and keep the remaining queries distinct. The one-to-one label assignment, (e.g. Hungarian matching) was first introduced to object detection by DETR [6]. Only one sample can be assigned to a corresponding ground truth object according to matching cost matrices, while all

other samples are assigned to background class. However, there exists a large number of similar queries which hinder training optimization. We use Intersection over Union (IoU) to measure the similarity of queries at the stage of one-to-one label assignment. If the IoU of two predict boxes is greater than the threshold, their corresponding queries are regarded as similar. Why only use IoU to measure the similarity of queries, rather than considering all matching cost matrices including IoU, L1 distance and Focal loss? There are two main reasons. First, the model adopts a one-to-one label assignment. Second, there are no ground truth objects with an IoU greater than a threshold close to 1, e.g. 0% ground truth objects with an IoU greater than 0.8 in the DIOR-R test set [38]. If a positive sample is assigned to an object, any other query with an IoU greater than the threshold is assigned as a background class. To quantify the similarity among queries, we conduct an analytical experiment on the DIOR-R test set shown in Fig. 4. Take threshold = 0.95 as an example, 4.00% of queries showed similarity in baseline model DDQ-O [12]. Our SDQ can significantly reduce the value to 0.74% which can prove the effectiveness of our method.

IV. EXPERIMENTS

A. Datasets

We conduct our experiments on five public datasets, including oriented object detection datasets DIOR-R [38], DOTA-v1.0 [8]/v1.5/v2.0 [49], and a horizontal object detection dataset MS COCO [9].

DIOR-R [38] is a large-scale oriented object detection dataset. It contains a total of 23463 remote sensing images and 192512 instances covering 20 common classes including windmill (WM), trainstation (TS), storagetank (STO), ship (SH), harbor (HA), golffield (GF), expressway toll station (ETS), bridge (BR), baseballfield (BF), airplane (APL), vehicle (VE), tennis court (TC), stadium (STA), overpass (OP), groundtrackfield (GTF), dam (DAM), expressway service area (ESA), chimney (CH), basketballcourt (BC) and airport (APO). We train our model on training and validation sets and report the results on the test set.

DOTA series including DOTA-v1.0/v1.5/v2.0 are used. DOTA-v1.0 [8] is designed for oriented object detection tasks which contain 188282 instances and 2806 remote sensing images ranging in size from 800×800 to 4000×4000. It covers 15 different object categories: Plane (PL), Baseball diamond (BD), Bridge (BR), Ground track field (GTF), Small vehicle (SV), Large vehicle (LV), Ship (SH), Tennis court (TC), Basketball court (BC), Storage tank (ST), Soccer-ball field (SBF), Roundabout (RA), Harbor (HA), Swimming pool (SP), and Helicopter (HC). DOTA-v1.5 uses the same images as DOTA-v1.0 but adds a new category Container Crane (CC) and more small instances, which contains 403318 instances. DOTA-v2.0 adds two categories Airport (Air) and Helipad (Heli) compared to DOTA-v1.5, which contains 11268 images and 1793658 instances. We use both training and validation sets for training and test set for testing for the DOTA series. The detection result of the test set is obtained by submitting testing results to DOTA’s official evaluation server.

TABLE II
COMPARISON WITH STATE-OF-THE-ART METHODS ON THE DIOR-R DATASET.

Method	APL	APO	BF	BC	BR	CH	DAM	ETS	ESA	GF	GTF	HA	OP	SH	STA	STO	TC	TS	VE	WM	mAP
<i>one-stage:</i>																					
RetinaNet-O [35]	61.49	28.52	73.57	81.17	23.98	72.54	19.94	72.39	58.20	69.25	79.54	32.14	44.87	77.71	67.57	61.09	81.46	47.33	38.01	60.24	57.55
Oriented Rep [39]	70.03	46.11	76.12	87.19	39.14	78.76	34.57	71.80	80.42	76.16	79.41	45.48	54.90	87.82	77.03	68.07	81.60	56.83	51.57	71.25	66.71
DCFL [1]	68.60	53.10	76.70	87.10	42.10	78.60	34.50	71.50	80.80	79.70	79.50	47.30	57.40	85.20	64.60	66.40	81.50	58.90	50.90	70.90	66.80
<i>two-stage:</i>																					
Faster RCNN-O [27]	62.79	26.80	71.72	80.91	34.20	72.57	18.95	66.45	65.75	66.63	79.24	34.95	48.79	81.14	64.34	71.21	81.44	47.31	50.46	65.21	59.54
Gliding Vertex [40]	65.35	28.87	74.96	81.33	33.88	74.31	19.58	70.72	64.70	72.30	78.68	37.22	49.64	80.22	69.26	61.13	81.49	44.76	47.71	65.04	60.06
RoI Transformer [34]	63.34	37.88	71.78	87.53	40.68	72.60	26.86	78.71	68.09	68.96	82.74	47.71	55.61	81.21	78.23	70.26	81.61	54.86	43.27	65.52	63.87
QPDet [41]	63.22	41.39	71.97	88.55	41.23	72.63	28.82	78.90	69.00	70.07	83.01	47.83	55.54	81.23	72.15	62.66	89.05	58.09	43.38	65.36	64.20
AOPG [38]	62.39	37.79	71.62	87.63	40.90	72.47	31.08	65.42	77.99	73.20	81.94	42.32	54.45	81.17	72.69	71.31	81.49	60.04	52.38	69.99	64.41
<i>end-to-end:</i>																					
ARS-DETR [42]	65.82	53.40	74.22	81.11	42.13	76.23	38.90	71.52	82.24	75.91	77.91	33.03	57.02	84.82	69.71	72.20	80.33	58.91	51.52	70.73	65.90
<i>end-to-end:</i>																					
RRoFormer	67.31	55.23	74.19	82.74	44.49	78.56	39.85	70.27	79.84	75.10	80.38	45.64	58.51	88.91	68.10	75.73	85.52	57.17	53.54	65.05	67.31

TABLE III
COMPARISON WITH STATE-OF-THE-ART METHODS ON THE DOTA-V1.0 DATASET. * DENOTES MULTI-SCALE TRAINING AND TESTING. *D. DETR* REPRESENTS DEFORMABLE DETR.

Method	Backbone	PL	BD	BR	GTF	SV	LV	SH	TC	BC	ST	SBF	RA	HA	SP	HC	mAP
<i>one-stage:</i>																	
R3Det [43]	R101	88.76	83.09	50.91	67.27	76.23	80.39	86.72	90.78	84.68	83.24	61.98	61.35	66.91	70.63	53.94	73.79
CFA [44]	R50	88.34	83.09	51.92	72.23	79.95	78.68	87.25	90.90	85.38	85.71	59.63	63.05	73.33	70.36	47.86	74.51
SASM [45]	R50	86.42	78.97	52.47	69.84	77.30	75.99	86.72	90.89	82.63	85.66	60.13	68.25	73.98	72.22	62.37	74.92
PSC [2]	R50	88.24	74.42	48.63	63.44	79.98	80.76	87.59	90.88	82.02	71.58	59.12	60.78	65.78	71.21	53.06	71.83
H2RBox [46]	R50	88.24	79.30	42.76	55.79	78.90	72.70	77.54	90.85	81.96	84.38	55.28	64.49	61.91	70.63	51.51	70.41
<i>two-stage:</i>																	
Mask OBB	R50	89.61	85.09	51.85	72.90	75.28	73.23	85.57	90.37	82.08	85.05	55.73	68.39	71.61	69.87	66.33	74.86
SCRDet [47]	R101	89.98	80.65	52.09	68.36	68.36	60.32	72.41	90.85	87.94	86.86	65.02	66.68	66.25	68.24	65.21	72.61
RoI Transformer [34]	R50	88.65	82.60	52.53	70.87	77.93	76.67	86.87	90.71	83.83	52.81	53.95	67.61	74.67	68.75	61.03	74.61
Gliding Vertex [40]	R101	89.64	85.00	52.26	77.34	73.01	73.14	86.82	90.74	79.02	86.81	59.55	70.91	72.94	70.86	57.32	75.02
Oriented R-CNN [3]	R50	89.46	82.12	54.78	70.86	78.93	83.00	88.20	90.90	87.50	84.68	63.97	67.69	74.94	68.84	52.28	75.87
<i>end-to-end:</i>																	
D. DETR-O [7]	R50	78.95	68.64	32.57	55.17	72.53	57.77	73.71	88.36	75.46	79.34	45.36	53.78	52.94	66.35	50.38	63.42
D. DETR-O w/ CSL [48]	R50	86.27	76.66	46.64	65.29	76.80	76.32	87.74	90.77	79.38	82.36	54.00	61.47	66.05	70.46	61.97	72.15
ARS-DETR [42]	R50	86.61	77.26	48.84	66.76	78.38	78.96	87.40	90.61	82.76	82.19	54.02	62.61	72.64	72.80	64.96	73.79
<i>end-to-end:</i>																	
RRoFormer	R50	87.45	78.57	47.36	69.01	79.58	81.27	88.53	90.89	82.80	86.21	58.68	64.20	75.21	74.44	61.39	75.04
RRoFormer*	R50	87.33	81.90	54.54	72.65	80.82	83.70	88.97	90.82	83.48	85.57	62.27	59.00	79.07	81.88	66.39	77.23

MS COCO 2017 [9] is a horizontal object detection dataset for natural scenes, consisting of 118K images as train2017 for training and 5K images as val2017 for validation. We train our model on train2017 and report the evaluation results on val2017.

B. Implementation Details

We select ResNet-50 [28] as the backbone which is pre-trained on the ImageNet [50]. We optimize the overall network with AdamW optimizer [51] with the warming up for 500 iterations. We use Focal loss [35] for classification and Rotated IoU/GIoU loss [36], [37] and L1 loss for regression.

For experiments on the DOTA-v1.5/v2.0, we use 2 NVIDIA RTX 2080ti with a batch size of 4 (2 images per GPU) and the learning rate of $5 \times e^{-5}$ for training, while a single GPU with a batch size of 2 and the learning rate of $2.5 \times e^{-5}$ on DOTA-v1.0 and DIOR-R. Models build on MMRotate [52] with Pytorch [53]. The weights of losses are 2.0, 2.0 and 5.0 for Focal loss, L1 loss and Rotated IoU loss respectively. Following official settings of the DOTA benchmark, we crop images into patches of 1024×1024 with overlaps of 200 and

train the model for 24 epochs. Images on DIOR-R are trained for 36 epochs with the original fixed size of 800×800 , while 12 epochs in ablation studies. To compare with other methods, the number of queries is 500, while in ablation studies on DIOR-R, it is 300.

For experiments on COCO 2017, we use 2 NVIDIA RTX 2080ti with a batch size of 4 (2 images per GPU) for training. Models build on MMDetection [54] with Pytorch. The weights of loss are 2.0, 5.0, and 2.0 for Focal loss, L1 loss, and IoU loss respectively. The learning rate is $2 \times e^{-5}$.

C. Main Results

Results on DIOR-R. As shown in Table II, our proposed RRoFormer is compared with CNN-based one-stage and two-stage detectors and transformer-based detectors. It achieves the state-of-the-art performance of 67.31% mAP with ResNet50 backbone on the DIOR-R benchmark. The backbones of all models are ResNet50 in Table II. Our method surpasses all comparison CNN-based one-stage and two-stage detectors and Transformer-based detectors. Overall, our method ob-

TABLE IV
COMPARISON WITH STATE-OF-THE-ART METHODS ON THE DOTA-v1.5 DATASET.

Method	PL	BD	BR	GTF	SV	LV	SH	TC	BC	ST	SBF	RA	HA	SP	HC	CC	mAP
<i>one-stage:</i>																	
RetinaNet-O [35]	71.43	77.64	42.12	64.65	44.53	56.79	73.31	90.84	76.02	59.96	46.95	69.24	59.65	64.52	48.06	0.83	59.16
DCFL [1]	-	-	-	-	56.72	-	80.87	-	-	75.65	-	-	-	-	-	-	67.37
<i>two-stage:</i>																	
Faster RCNN-O [27]	71.89	74.47	44.45	59.87	51.28	68.98	79.37	90.78	77.38	67.50	47.75	69.72	61.22	65.28	60.47	1.54	62.00
Mask R-CNN [55]	76.84	73.51	49.90	57.80	51.31	71.34	79.75	90.46	74.21	66.07	46.21	70.61	63.07	64.46	57.81	9.42	62.67
HTC [56]	77.80	73.67	51.40	63.99	51.54	73.31	80.31	90.48	75.12	67.34	48.51	70.63	64.84	64.48	55.87	5.15	63.40
ReDet [4]	79.20	82.81	51.92	71.41	52.38	75.73	80.92	90.83	75.81	68.64	49.29	72.03	73.36	70.55	63.33	11.53	66.86
<i>end-to-end:</i>																	
RRoFormer	78.44	75.43	48.84	63.62	62.16	78.41	88.94	90.84	75.29	81.83	57.05	66.44	73.95	72.69	51.64	13.37	67.43

TABLE V
COMPARISON WITH STATE-OF-THE-ART METHODS ON THE DOTA-v2.0 DATASET.

Method	Plane	BD	Bridge	GTF	SV	LV	Ship	TC	BC	ST	SBF	RA	Harbor	SP	HC	CC	Air	Heli	mAP
<i>one-stage:</i>																			
SASM [45]	70.30	40.62	37.01	59.03	40.21	45.46	44.60	78.58	49.34	60.73	29.89	46.57	42.95	48.31	28.13	1.82	76.37	0.74	44.53
Oriented Rep [39]	73.02	46.68	42.37	63.05	47.06	50.28	58.64	78.84	57.12	66.77	35.21	50.76	48.77	51.62	34.23	6.17	64.66	5.87	48.95
ATSS-O [26]	77.46	49.55	42.12	62.61	45.15	48.40	51.70	78.43	59.33	62.65	39.18	52.43	42.92	53.98	42.70	5.91	67.09	10.68	49.57
DCFL [1]	75.71	49.40	44.69	63.23	46.48	51.55	55.50	79.30	59.96	65.39	41.86	54.42	47.03	55.72	50.49	11.75	69.01	7.75	51.57
<i>two-stage:</i>																			
Mask R-CNN [55]	76.20	49.91	41.61	60.00	41.08	50.77	56.24	78.01	55.85	57.48	36.62	51.67	47.39	55.79	59.06	3.64	60.26	8.95	49.47
HTC [56]	77.69	47.25	41.15	60.71	41.77	52.79	58.87	78.74	55.22	58.49	38.57	52.48	49.58	56.18	54.09	4.20	66.38	11.92	50.34
RoI Transformer [34]	71.81	48.39	45.88	64.02	42.09	54.39	59.92	82.70	63.29	58.71	41.04	52.82	53.32	56.18	57.94	25.71	63.72	8.70	52.81
Oriented R-CNN [3]	77.95	50.29	46.73	65.24	42.61	54.56	60.02	79.08	61.69	59.42	42.26	56.89	51.11	56.16	59.33	25.81	60.67	9.17	53.28
<i>end-to-end:</i>																			
RRoFormer	77.58	49.96	38.60	53.82	54.97	57.12	68.93	77.88	59.59	71.92	40.17	51.22	53.00	57.12	49.66	25.42	66.92	5.17	53.28

tains 0.51%, 2.9%, and 1.41% improvements in mAP over DCFL [1], AOPG [38], and ARS-DETR [42].

Results on DOTA-v1.0. We compare our RRoFormer method with modern CNN-based one-stage and two-stage detectors and transformer-based detectors. Table III reports the detailed results of every category on the DOTA-v1.0 dataset. With ResNet50 as the backbone, RRoFormer obtains 75.04% mAP under single-scale training and testing. In addition, with the multi-scale training augmentation strategy, our method achieves 77.23% mAP using the ResNet50 backbone. RRoFormer surpasses most comparison methods, particularly compared to Transformer-based detectors.

Results on DOTA-v1.5. We report results on DOTA-v1.5 in Table IV compared with current CNN-based one-stage and two-stage detectors. The backbones of all models are ResNet50 in Table IV. Our method achieves 67.43% mAP which achieves state-of-the-art performance under single-scale training and testing. Especially for the categories with small instances (e.g., HA, SP, CC), it performs better.

Results on DOTA-v2.0. Table V shows a comparison of our method with the modern detectors on the DOTA-v2.0 dataset. The backbones of all models are ResNet50 in Table V. Our proposed method achieves the new state-of-the-art performance of 53.28% mAP under single-scale training and testing. It is comparable to the mAP of the previous best models Oriented R-CNN [3].

D. Effects of Selective Distinct Queries

To verify the effectiveness of our proposed Selective Distinct Queries module, we apply the SDQ to a horizontal object detector Sparse R-CNN [13] with the ResNet50 backbone. The model is trained and tested on COCO 2017 and detailed results

TABLE VI
RESULTS FOR SDQ APPLIED TO SPARSE R-CNN.

Model	w/SDQ	#query	#epochs	mAP	FPS	Params(M)
Sparse R-CNN		100	12	37.9	20.6	106
	✓	100	12	41.0 (+3.1)	20.0	106
		300	36	45.0	20.5	106
	✓	300	36	46.8 (+1.8)	19.3	106

TABLE VII
ABLATION STUDY OF THE EFFECTS OF PROPOSED INDIVIDUAL STRATEGY.

Method	RRoI attn	SDQ	mAP	Params(M)	FPS
baseline			61.66	64	13.4
RRoFormer	✓		61.67	41	13.9
		✓	62.76	41	14.1

are reported in table VI. We collect selective queries from only 5th decoder layer with a total of 6 decoder layers. Then we obtain distinct queries also in front of the last decoder layers and the IoU threshold is set to 0.7. With 100 queries and 12 training epochs, SDQ significantly improves +3.1% mAP compared with the baseline. Increasing the number of queries to 300 and training epoch to 36, SDQ achieves 46.8% (+1.8%) mAP on the COCO val2017 set with the help of a random resize augmentation strategy from DETR [6]. These experiments can fully prove the effectiveness of the SDQ method. The SDQ would not bring extra parameters of the model and FPS is only slightly reduced (20.0 vs 20.6).

E. Ablation Study

Effects of Individual Strategy. We check the effectiveness of each proposed strategy in the proposed method. As shown in table VII, the baseline detector DDQ-O [12] yields a result

TABLE VIII
DIFFERENT NUMBER OF ATTENTION HEADS OF RRoI ATTENTION.

Head	2	4	8	16
mAP	61.36	62.19	62.63	55.63

TABLE IX
DIFFERENT POOLING SIZE OF RRoI ATTENTION.

Pooling Size	5	7	9
mAP	61.35	62.63	62.32

TABLE X
ABLATION STUDY OF DIFFERENT IOU THRESHOLD FOR SDQ.

threshold	0.8	0.85	0.9	0.95
mAP	62.58	62.76	62.63	62.49

TABLE XI
ABLATION STUDY OF DIFFERENT DECODER LAYER IN SELECTIVE DISTINCT QUERIES.

Method	Layers	Selective	Distinct	AP
SDQ	3	$0^{th}, 1^{st}, 2^{nd}$	2^{nd}	58.01
		$1^{st}, 2^{nd}$	2^{nd}	60.66
		1^{st}	1^{st}	58.03
		2^{nd}	2^{nd}	62.08

of 61.66% mAP on DIOR-R with 300 queries. When we gradually apply the RRoI attention and SDQ into the baseline detector, our model achieves 61.67% and 62.76% mAP respectively, verifying the effectiveness of each design. RRoI attention significantly reduces the parameters by 23 million compared to dynamic interaction in the baseline detectors. When applying RRoI attention to the baseline model, due to the reduction in parameters, the FPS increases by 0.5. When we further apply SDQ, since there are fewer distinct queries than the initial queries, the FPS increases slightly by 0.2.

The number of attention head. Following deformable attention [7], our RRoI attention also adopts multiple heads. Different heads establish different associations between queries and values. In this ablation, we use different numbers of m heads. As we increase the number of heads from 2 to 8, the mAP grows from 61.36% to 62.63% on DIOR-R, shown in Table VIII. This indicates that the multi-head attention extends the ability to focus on different parts of features, and provides multiple subspaces for representation. When we increase the number of heads to 16, there is a decline in performance. We suspect that the redundant head focuses on redundant features.

Different pooling size. To further explore RRoI Attention, we adopt different pooling sizes r . As the pooling size r increases, more features will be highlighted in oriented boxes. When pooling size r is set to 5, the AP is only 61.35% on DIOR-R, shown in Table IX. When it is increased to 7, the mAP can achieve 62.63%. This suggests that abundant features are sufficient to represent objects. When we increase the pooling size to 9, the performance of model declines. It indicates that redundant features confuse the attention mechanism.

Threshold of Selective Distinct Queries. To further explore the effectiveness of SDQ, we conducted ablation experiments

TABLE XII
ABLATION STUDY OF REDUCING THE DECODER LAYERS.

Method	Layers	Selective	Distinct	AP
SDQ	3	2^{nd}	2^{nd}	62.08
	2	1^{st}	1^{st}	62.63
	1	0^{th}	0^{th}	44.02

TABLE XIII
ABLATION STUDY OF DIFFERENT QUERY SELECTION MECHANISM.

Method	Layers	Selective	Distinct	AP
Top-k	3	$1^{st}, 2^{nd}$	2^{nd}	59.49
Stack				59.99
SDQ				60.66

on the different IoU thresholds shown in table X. To filter the similar queries and keep the remaining queries distinct, the threshold is a high value close to 1 in SDQ. As the IoU threshold value increases from 0.8 to 0.85, the mAP increases by 0.18% on DIOR-R. When the IoU threshold increases to 0.95 which is very close to 1, the mAP value decreases slightly, indicating that there are very few predicted boxes that fully coincide or are close to perfectly coinciding.

Different decoder layers in Selective Distinct Queries. To further verify the effectiveness of SDQ, we performed ablation experiments with different numbers of decoder layers in SDQ on DIOR-R, shown in table XI. The total number of decoder layers is 3 here. When we collect queries from the 2^{nd} decoder layer as selective queries and filter similar queries to obtain distinct queries also at the 2^{nd} layer, the model achieves the best 62.08% mAP on DIOR-R. When selective queries contain more queries from front layers, e.g. initial queries, there is a significant decline in performance. Queries at the front layers can not adequately represent objects.

Reduce total decoder layers. To further verify the effectiveness of SDQ, we performed ablation experiments on reducing the total decoder layers on DIOR-R, shown in Table XII. When only one decoder layer, we do SDQ on initial queries. In this condition, our method only achieves 44.02% mAP. When we increase the number of decoder layers from 2 to 3, the mAP drops from 62.63% to 62.08%. The decoder and attention bring too many parameters which may be redundant.

Queries selection mechanism. To further verify the effectiveness of SDQ, we performed ablation experiments with different selection mechanisms on DIOR-R, including top- k and stack mechanisms, shown in table XIII. Following DINO [10], we choose top- k queries according to scores of multi-class classification, while in Deformable DETR [7], the top- k method selects proposals only according to scores of binary classification. In the top- k mechanism, we collect queries from 1^{st} and 2^{nd} decoder layers and choose top- k queries at 2^{nd} layer. The number of k is equal to initial queries. In addition, we densely stack queries from 1^{st} and 2^{nd} decoder layers to 3^{th} layers which can be regarded as a revision of SQR [22]. The number of queries multiplies many times according to candidate layers through the stack. Essentially, the method of stack increases performance by

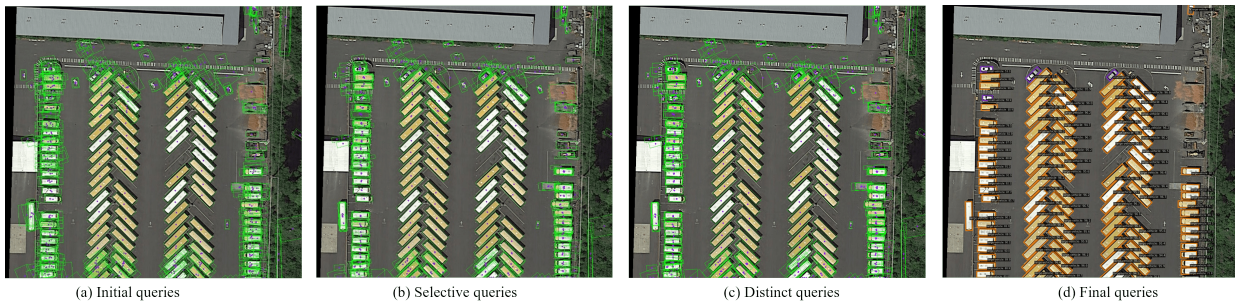


Fig. 5. Visualization of different queries in decoder. (a) Initial queries. (b) Selective queries. (c) Distinct queries. (d) Final queries.

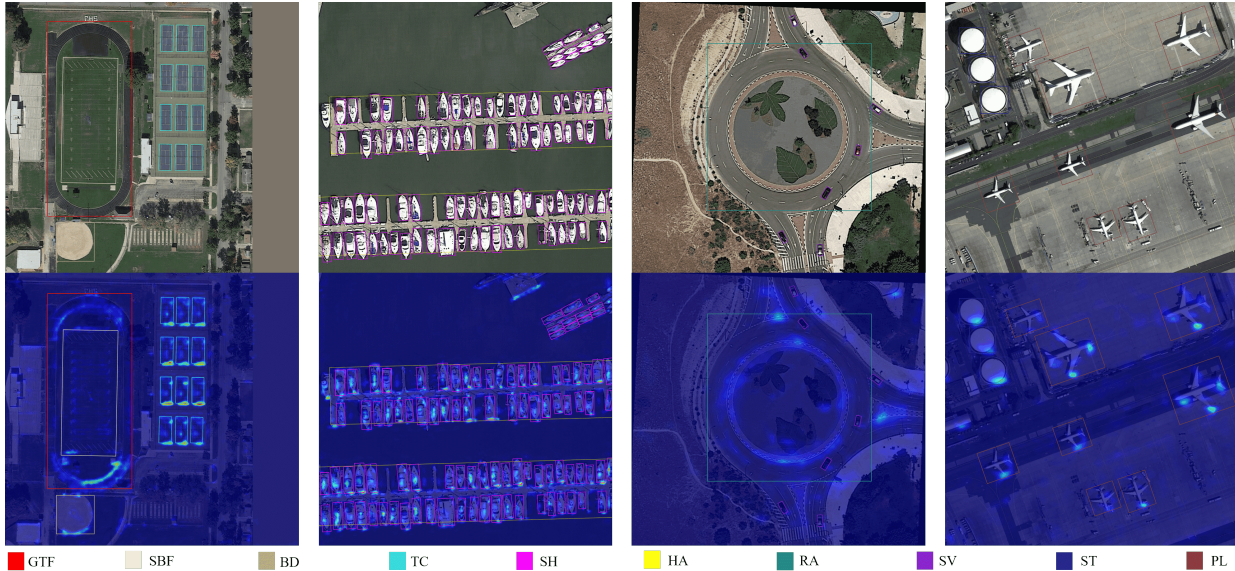


Fig. 6. Some detection results on DOTA-v1.0. The first row of images shows the detection results. The second row of images shows RRoi attention.



Fig. 7. Some detection results on DIOR-R .

increasing the number of queries. For a fair comparison, our SDQ also collects selective queries from 1st and 2nd decoder layers. Compared with the other two different methods, our SDQ mechanism is the most effective and is the only one that can reduce the number of queries.

F. visualization

Visualization of queries through Selective Distinct Queris. Shown in Fig. 5, we visualize initial queries, selective queries, distinct queries, and final queries. Initial queries are more random. Selective queries are more accurate than initial queries. We filter similar queries to obtain distinct queries. Final queries can detect objects accurately.

Visualization of RRoi attention We visualize RRoi attention in Fig. 6 without using CAM [57]. We observe that it

mostly focuses on object extremities such as the front and back of planes and ships. These highlighted areas are very similar to DETR [6] and Deformable DETR [7].

Visualization of results We visualize some predicted results in Fig. 6 and Fig. 7. We can see that our model detects objects accurately.

V. CONCLUSIONS

In this paper, we propose an end-to-end detector for oriented object detection in remote sensing images, including two key technologies RRoi attention and SDQ. The proposed RRoi attention align image features and oriented boxes through a cross-attention mechanism for objects with arbitrary orientations and varying scales. To avoid a large number of initial queries or extra auxiliary branches and eliminate the similar

queries hindering the optimization, the SDQ first collects high-quality selective queries from intermediate decoder layers, and second filters similar queries to keep remaining queries distinct which facilitates the one-to-one label assignment. Extensive experiments show that our method has competitive accuracy to the modern CNN-based one-stage and two-stage detectors and transformer-based detectors. We hope it will inspire researchers to further explore the application of end-to-end models in oriented object detection.

REFERENCES

- [1] C. Xu, J. Ding, J. Wang, W. Yang, H. Yu, L. Yu, and G.-S. Xia, "Dynamic coarse-to-fine learning for oriented tiny object detection," in *Proceedings of the IEEE/CVF Conference on Computer Vision and Pattern Recognition*, 2023, pp. 7318–7328.
- [2] Y. Yu and F. Da, "Phase-shifting coder: Predicting accurate orientation in oriented object detection," in *Proceedings of the IEEE/CVF Conference on Computer Vision and Pattern Recognition*, 2023, pp. 13 354–13 363.
- [3] X. Xie, G. Cheng, J. Wang, X. Yao, and J. Han, "Oriented r-cnn for object detection," in *Proceedings of the IEEE/CVF international conference on computer vision*, 2021, pp. 3520–3529.
- [4] J. Han, J. Ding, N. Xue, and G.-S. Xia, "Redet: A rotation-equivariant detector for aerial object detection," in *Proceedings of the IEEE/CVF Conference on Computer Vision and Pattern Recognition*, 2021, pp. 2786–2795.
- [5] A. Vaswani, N. Shazeer, N. Parmar, J. Uszkoreit, L. Jones, A. N. Gomez, Ł. Kaiser, and I. Polosukhin, "Attention is all you need," *Advances in neural information processing systems*, vol. 30, 2017.
- [6] N. Carion, F. Massa, G. Synnaeve, N. Usunier, A. Kirillov, and S. Zagoruyko, "End-to-end object detection with transformers," in *European conference on computer vision*. Springer, 2020, pp. 213–229.
- [7] X. Zhu, W. Su, L. Lu, B. Li, X. Wang, and J. Dai, "Deformable detr: Deformable transformers for end-to-end object detection," in *International Conference on Learning Representations*, 2020.
- [8] G.-S. Xia, X. Bai, J. Ding, Z. Zhu, S. Belongie, J. Luo, M. Datcu, M. Pelillo, and L. Zhang, "Dota: A large-scale dataset for object detection in aerial images," in *Proceedings of the IEEE conference on computer vision and pattern recognition*, 2018, pp. 3974–3983.
- [9] T.-Y. Lin, M. Maire, S. Belongie, J. Hays, P. Perona, D. Ramanan, P. Dollár, and C. L. Zitnick, "Microsoft coco: Common objects in context," in *Computer Vision—ECCV 2014: 13th European Conference, Zurich, Switzerland, September 6–12, 2014, Proceedings, Part V 13*. Springer, 2014, pp. 740–755.
- [10] H. Zhang, F. Li, S. Liu, L. Zhang, H. Su, J. Zhu, L. Ni, and H. Shum, "Dino: Detr with improved denoising anchor boxes for end-to-end object detection. arxiv 2022," *arXiv preprint arXiv:2203.03605*, 2022.
- [11] D. Jia, Y. Yuan, H. He, X. Wu, H. Yu, W. Lin, L. Sun, C. Zhang, and H. Hu, "Dets with hybrid matching," in *Proceedings of the IEEE/CVF Conference on Computer Vision and Pattern Recognition*, 2023, pp. 19 702–19 712.
- [12] S. Zhang, X. Wang, J. Wang, J. Pang, C. Lyu, W. Zhang, P. Luo, and K. Chen, "Dense distinct query for end-to-end object detection," in *Proceedings of the IEEE/CVF Conference on Computer Vision and Pattern Recognition*, 2023, pp. 7329–7338.
- [13] P. Sun, R. Zhang, Y. Jiang, T. Kong, C. Xu, W. Zhan, M. Tomizuka, L. Li, Z. Yuan, C. Wang *et al.*, "Sparse r-cnn: End-to-end object detection with learnable proposals," in *Proceedings of the IEEE/CVF conference on computer vision and pattern recognition*, 2021, pp. 14 454–14 463.
- [14] Z. Zong, G. Song, and Y. Liu, "Dets with collaborative hybrid assignments training," in *Proceedings of the IEEE/CVF International Conference on Computer Vision*, 2023, pp. 6748–6758.
- [15] P. Gao, M. Zheng, X. Wang, J. Dai, and H. Li, "Fast convergence of detr with spatially modulated co-attention," in *Proceedings of the IEEE/CVF international conference on computer vision*, 2021, pp. 3621–3630.
- [16] Y. Wang, X. Zhang, T. Yang, and J. Sun, "Anchor detr: Query design for transformer-based detector," in *Proceedings of the AAAI conference on artificial intelligence*, vol. 36, no. 3, 2022, pp. 2567–2575.
- [17] X. Dai, Y. Chen, J. Yang, P. Zhang, L. Yuan, and L. Zhang, "Dynamic detr: End-to-end object detection with dynamic attention," in *Proceedings of the IEEE/CVF International Conference on Computer Vision*, 2021, pp. 2988–2997.
- [18] J. Hu, L. Huang, T. Ren, S. Zhang, R. Ji, and L. Cao, "You only segment once: Towards real-time panoptic segmentation," in *Proceedings of the IEEE/CVF Conference on Computer Vision and Pattern Recognition*, 2023, pp. 17 819–17 829.
- [19] B. Yang, G. Bender, Q. V. Le, and J. Ngiam, "Condconv: Conditionally parameterized convolutions for efficient inference," *Advances in neural information processing systems*, vol. 32, 2019.
- [20] Y. Chen, X. Dai, M. Liu, D. Chen, L. Yuan, and Z. Liu, "Dynamic convolution: Attention over convolution kernels," in *Proceedings of the IEEE/CVF conference on computer vision and pattern recognition*, 2020, pp. 11 030–11 039.
- [21] Q. Hong, F. Liu, D. Li, J. Liu, L. Tian, and Y. Shan, "Dynamic sparse r-cnn," in *Proceedings of the IEEE/CVF conference on computer vision and pattern recognition*, 2022, pp. 4723–4732.
- [22] F. Chen, H. Zhang, K. Hu, Y.-K. Huang, C. Zhu, and M. Savvides, "Enhanced training of query-based object detection via selective query recollection," in *Proceedings of the IEEE/CVF Conference on Computer Vision and Pattern Recognition*, 2023, pp. 23 756–23 765.
- [23] Y. Cui, L. Yang, and H. Yu, "Learning dynamic query combinations for transformer-based object detection and segmentation," in *Proceedings of the 40th International Conference on Machine Learning*, ser. ICML'23. JMLR.org, 2023.
- [24] Q. Chen, X. Chen, J. Wang, S. Zhang, K. Yao, H. Feng, J. Han, E. Ding, G. Zeng, and J. Wang, "Group detr: Fast detr training with group-wise one-to-many assignment," in *Proceedings of the IEEE/CVF International Conference on Computer Vision*, 2023, pp. 6633–6642.
- [25] F. Li, H. Zhang, S. Liu, J. Guo, L. M. Ni, and L. Zhang, "Dn-detr: Accelerate detr training by introducing query denoising," in *Proceedings of the IEEE/CVF Conference on Computer Vision and Pattern Recognition*, 2022, pp. 13 619–13 627.
- [26] S. Zhang, C. Chi, Y. Yao, Z. Lei, and S. Z. Li, "Bridging the gap between anchor-based and anchor-free detection via adaptive training sample selection," in *Proceedings of the IEEE/CVF conference on computer vision and pattern recognition*, 2020, pp. 9759–9768.
- [27] S. Ren, K. He, R. Girshick, and J. Sun, "Faster r-cnn: Towards real-time object detection with region proposal networks," *Advances in neural information processing systems*, vol. 28, 2015.
- [28] K. He, X. Zhang, S. Ren, and J. Sun, "Deep residual learning for image recognition," in *Proceedings of the IEEE conference on computer vision and pattern recognition*, 2016, pp. 770–778.
- [29] Z. Liu, Y. Lin, Y. Cao, H. Hu, Y. Wei, Z. Zhang, S. Lin, and B. Guo, "Swin transformer: Hierarchical vision transformer using shifted windows," in *Proceedings of the IEEE/CVF international conference on computer vision*, 2021, pp. 10 012–10 022.
- [30] Y. Lin, Y. Yuan, Z. Zhang, C. Li, N. Zheng, and H. Hu, "Detr does not need multi-scale or locality design," in *Proceedings of the IEEE/CVF International Conference on Computer Vision*, 2023, pp. 6545–6554.
- [31] W. Lv, S. Xu, Y. Zhao, G. Wang, J. Wei, C. Cui, Y. Du, Q. Dang, and Y. Liu, "Dets beat yolos on real-time object detection," *arXiv preprint arXiv:2304.08069*, 2023.
- [32] F. Li, A. Zeng, S. Liu, H. Zhang, H. Li, L. Zhang, and L. M. Ni, "Lite detr: An interleaved multi-scale encoder for efficient detr," in *Proceedings of the IEEE/CVF Conference on Computer Vision and Pattern Recognition*, 2023, pp. 18 558–18 567.
- [33] Z. Gao, L. Wang, B. Han, and S. Guo, "Adamixer: A fast-converging query-based object detector," in *Proceedings of the IEEE/CVF Conference on Computer Vision and Pattern Recognition*, 2022, pp. 5364–5373.
- [34] J. Ding, N. Xue, Y. Long, G.-S. Xia, and Q. Lu, "Learning roi transformer for oriented object detection in aerial images," in *Proceedings of the IEEE/CVF Conference on Computer Vision and Pattern Recognition*, 2019, pp. 2849–2858.
- [35] T.-Y. Lin, P. Goyal, R. Girshick, K. He, and P. Dollár, "Focal loss for dense object detection," in *Proceedings of the IEEE international conference on computer vision*, 2017, pp. 2980–2988.
- [36] D. Zhou, J. Fang, X. Song, C. Guan, J. Yin, Y. Dai, and R. Yang, "Iou loss for 2d/3d object detection," in *2019 international conference on 3D vision (3DV)*. IEEE, 2019, pp. 85–94.
- [37] H. Rezaatofghi, N. Tsoi, J. Gwak, A. Sadeghian, I. Reid, and S. Savarese, "Generalized intersection over union: A metric and a loss for bounding box regression," in *Proceedings of the IEEE/CVF conference on computer vision and pattern recognition*, 2019, pp. 658–666.
- [38] G. Cheng, J. Wang, K. Li, X. Xie, C. Lang, Y. Yao, and J. Han, "Anchor-free oriented proposal generator for object detection," *IEEE Transactions on Geoscience and Remote Sensing*, vol. 60, pp. 1–11, 2022.
- [39] W. Li, Y. Chen, K. Hu, and J. Zhu, "Oriented reppoints for aerial object detection," in *Proceedings of the IEEE/CVF conference on computer vision and pattern recognition*, 2022, pp. 1829–1838.

- [40] Y. Xu, M. Fu, Q. Wang, Y. Wang, K. Chen, G.-S. Xia, and X. Bai, "Gliding vertex on the horizontal bounding box for multi-oriented object detection," *IEEE transactions on pattern analysis and machine intelligence*, vol. 43, no. 4, pp. 1452–1459, 2020.
- [41] Y. Yao, G. Cheng, G. Wang, S. Li, P. Zhou, X. Xie, and J. Han, "On improving bounding box representations for oriented object detection," *IEEE Transactions on Geoscience and Remote Sensing*, vol. 61, pp. 1–11, 2022.
- [42] Y. Zeng, X. Yang, Q. Li, Y. Chen, and J. Yan, "Ars-detr: Aspect ratio sensitive oriented object detection with transformer," *arXiv preprint arXiv:2303.04989*, 2023.
- [43] X. Yang, J. Yan, Z. Feng, and T. He, "R3det: Refined single-stage detector with feature refinement for rotating object," in *Proceedings of the AAAI conference on artificial intelligence*, vol. 35, no. 4, 2021, pp. 3163–3171.
- [44] Z. Guo, C. Liu, X. Zhang, J. Jiao, X. Ji, and Q. Ye, "Beyond bounding-box: Convex-hull feature adaptation for oriented and densely packed object detection," in *Proceedings of the IEEE/CVF conference on Computer Vision and Pattern Recognition*, 2021, pp. 8792–8801.
- [45] L. Hou, K. Lu, J. Xue, and Y. Li, "Shape-adaptive selection and measurement for oriented object detection," in *Proceedings of the AAAI Conference on Artificial Intelligence*, vol. 36, no. 1, 2022, pp. 923–932.
- [46] X. Yang, G. Zhang, W. Li, Y. Zhou, X. Wang, and J. Yan, "H2rbox: Horizontal box annotation is all you need for oriented object detection," in *The Eleventh International Conference on Learning Representations*, 2022.
- [47] X. Yang, J. Yang, J. Yan, Y. Zhang, T. Zhang, Z. Guo, X. Sun, and K. Fu, "Scrdet: Towards more robust detection for small, cluttered and rotated objects," in *Proceedings of the IEEE/CVF international conference on computer vision*, 2019, pp. 8232–8241.
- [48] X. Yang and J. Yan, "Arbitrary-oriented object detection with circular smooth label," in *Computer Vision—ECCV 2020: 16th European Conference, Glasgow, UK, August 23–28, 2020, Proceedings, Part VIII 16*. Springer, 2020, pp. 677–694.
- [49] J. Ding, N. Xue, G.-S. Xia, X. Bai, W. Yang, M. Y. Yang, S. Belongie, J. Luo, M. Datcu, M. Pelillo *et al.*, "Object detection in aerial images: A large-scale benchmark and challenges," *IEEE transactions on pattern analysis and machine intelligence*, vol. 44, no. 11, pp. 7778–7796, 2021.
- [50] J. Deng, W. Dong, R. Socher, L.-J. Li, K. Li, and L. Fei-Fei, "Imagenet: A large-scale hierarchical image database," in *2009 IEEE conference on computer vision and pattern recognition*. Ieee, 2009, pp. 248–255.
- [51] I. Loshchilov and F. Hutter, "Decoupled weight decay regularization," in *International Conference on Learning Representations*, 2018.
- [52] Y. Zhou, X. Yang, G. Zhang, J. Wang, Y. Liu, L. Hou, X. Jiang, X. Liu, J. Yan, C. Lyu *et al.*, "Mmrotate: A rotated object detection benchmark using pytorch," in *Proceedings of the 30th ACM International Conference on Multimedia*, 2022, pp. 7331–7334.
- [53] A. Paszke, S. Gross, F. Massa, A. Lerer, J. Bradbury, G. Chanan, T. Killeen, Z. Lin, N. Gimelshein, L. Antiga *et al.*, "Pytorch: An imperative style, high-performance deep learning library," *Advances in neural information processing systems*, vol. 32, 2019.
- [54] K. Chen, J. Wang, J. Pang, Y. Cao, Y. Xiong, X. Li, S. Sun, W. Feng, Z. Liu, J. Xu *et al.*, "Mmdetection: Open mmlab detection toolbox and benchmark," *arXiv preprint arXiv:1906.07155*, 2019.
- [55] K. He, G. Gkioxari, P. Dollár, and R. Girshick, "Mask r-cnn," in *Proceedings of the IEEE international conference on computer vision*, 2017, pp. 2961–2969.
- [56] K. Chen, J. Pang, J. Wang, Y. Xiong, X. Li, S. Sun, W. Feng, Z. Liu, J. Shi, W. Ouyang *et al.*, "Hybrid task cascade for instance segmentation," in *Proceedings of the IEEE/CVF conference on computer vision and pattern recognition*, 2019, pp. 4974–4983.
- [57] B. Zhou, A. Khosla, A. Lapedriza, A. Oliva, and A. Torralba, "Learning deep features for discriminative localization," in *Proceedings of the IEEE conference on computer vision and pattern recognition*, 2016, pp. 2921–2929.